

Final report

Project: NN OTKA-112156 „New type functional alloy films”.

The project started on the 1st of February 2015 with certain difficulties due to transition of the Institute (MFA) from the Centre for Natural Sciences to the Centre for Energy Research. Simultaneously there was a substantial delay in the relocation of project contract and financial support to the new host institute. These problems were solved by the end of year 2015.

The main goal of the project was to reveal the structural development and the relation between structure and properties of two- and multicomponent and HEA (High Entropy Alloy) thin films prepared by magnetron sputtering but also other techniques.

The project was carried out in international co-operation, the co-operating partner being prof. Diederik Depla, and his colleagues at Ghent Technical University, Belgium.

1. Phase separation in alloy nanoparticles (Cu-Ag) [1].

The project started with the investigation of phase separation mechanisms in alloys of non-mixing components. The model experiments were thought for the two-component Cu-Ag system. It was an important question how and what kind of phase separation processes take place during the initial stages of film formation. It was established that below 5 nm particle size no phase separation occurs. In the concentration region of 15-80 at. % Ag phase separation was observed in alloy particles of 15 and 30 at. % Ag above 5 nm particle size (obtained in a BSc diploma by Eszter Bokányi, Roland Eötvös University, 2014, supervisor Fanni Misják). The basic result contributing to the present project is that the process of phase separation is spinodal decomposition, which occurs depending on the size and composition of the particle. Measuring the variation of lattice parameters in HREM images of individual particles we determined also the width of the miscibility gap in the 30 at% Ag nanoparticles. The average width of the gap is 85-89 at%. However, in a few individual particles smaller gap widths were also detected (down to 70 at%). Phase separation in particles undergoing incomplete coalescence occurs even when the size of coalescing grains is below 5 nm. In higher Ag content films (60-80 at. %) no phase-separation is observed until coalescence sets in (about 10 nm of particle size). The size dependence of phase separation was explained by the composition dependence of the critical (Cahn-Hilliard) spinodal wavelength, suggesting that the critical particle size, below which no phase separation occurs, equals to this wavelength. In co-operation with Zoltan Erdélyi (Debrecen University) the composition dependence of the critical wavelength of compositional oscillations was calculated. It gave 6 nm for the critical size for 30 at. % Ag content particles and a size of 8 nm for 60 at. % of Ag [1]. The results correlate fairly well with the critical sizes, obtained experimentally (fig. 1). Computer simulations by Stochastic Kinetic Mean-Field model confirmed the size-dependence and resulted in atomic structures that are similar to the experimental observations [9].

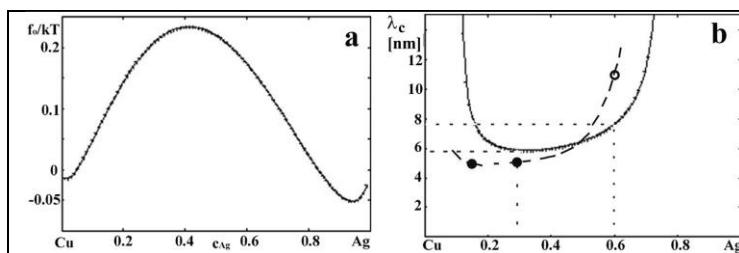


Figure. 1. Homogeneous part of the Gibbs free energy f_0 (a) and critical wavelength λ_c in spinodal decomposition (b) versus composition in Cu-Ag system. In (b) full dots mark experimental critical size, the open circle marks the estimated lower value of the critical size [1].

2. The structure of the basic HEA alloy, effect of contaminants and growth temperature [4].

The five component CoCrFeNiCu (HEA) films were deposited by DC magnetron sputtering using spark-melted targets at a background pressure of 5×10^{-6} Pa, with a deposition rate of ~ 10 nm/min. The working pressure was 0.3 Pa by applying 99.9 % pure argon as sputtering gas. The films were deposited onto oxidized (100) Si wafers. The growth was carried out at room temperature as well as at 200 and 380°C.

The structure of the films grown at room temperature (Fig. 2a) is single phase face-centred cubic (FCC, $a=0.36$ nm) and corresponds to zone T structure, with a well expressed $\langle 111 \rangle$ texture. The width of the columns is rather uniform about ~ 25 -50 nm and the growth competition region is about 50 nm thick in the 500 nm thick film. The columns are rather defective, the main defects being planar defects. The films grown at high temperature (Fig. 2c) possess also the single phase FCC structure; from HREM measurements local ordering and formation of (nano)compound phases could be deduced. The morphology is at transition between zones II and III. This is also supported by the random crystallographic orientation of the grains [4].

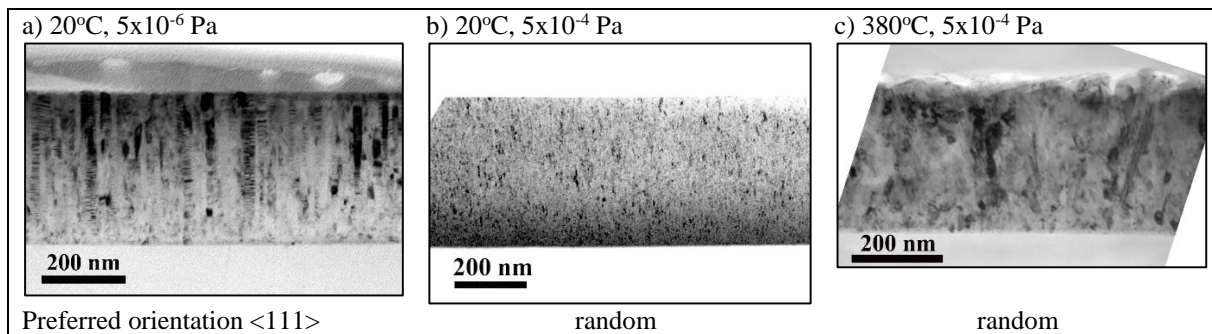


Figure 2. Cross section TEM images of HEA films grown at different growth temperatures and base pressures.

When the five component CoCrFeNiCu (HEA) films were deposited at the base pressure in the vacuum chamber 5×10^{-4} Pa (Fig. 2b) with a deposition rate of 10 nm/min, corresponding to a metallic flux of approximately 1.40×10^{15} at/cm²s a zone III type microstructure formed. The average gaseous impurity flux corresponded to 1.42×10^{15} at/cm²s. Hence, this (HEA) film was deposited with an average impurity-to-metal flux ratio of about 1. This shows that the CoCrCuFeNi film was grown in the impurity-controlled conditions which involves the formation of covering layers on the growth surface and repeated nucleation of the crystalline (HEA) phase in the thickness of the film. The consequence of this growth mechanism is the formation of a nano-size grain structure (about 10 nm) and the lack of crystallographic texture. As a result, the main processes being active in the film formation are: Nucleation and growth of the FCC (HEA) phase, the formation of a covering layer– presumably oxide, repeated nucleation of the (HEA) phase on the surface of covering layer.

Thermal stability of the basic alloy (equiatomic CrFeCoNiCu) has been studied by in-situ annealing experiments in the electron microscope [11]. The advantage of this investigation is that the ongoing changes during heating can be observed and recorded in real time. The films were annealed from 20°C up to 700°C. During the annealing procedure (50°C steps in each 5

min) the vacuum in the microscope was maintained in the $(4-6)\times 10^{-7}$ mbar for the whole annealing time (about 60 min). Isothermal annealing at 450 and 550°C were also carried out. The CrFeCoNiCu HEA alloy films were stable in their FCC structure up to 400°C. At 450°C a HEA BCC phase appeared in the film. This change was considered to occur by a diffusionless phase transformation. The structure, composition and grain size of the newly formed BCC grains corresponded to the HEA FCC grains. The separation of the components began above 550°C. The actual activation energy of this process was estimated to be around 160 kJ/mol. It must be related to lattice diffusion in the HEA alloy, which should be the rate limiting process during transformations above 550°C. These transformations were: Formation of a new phase with a large unit cell, epitaxial to the already formed BCC phase. The cell parameters correspond to $2\times 2\times 4$ units of the BCC cell. The crystals composed mainly from Cr (about 80 at. %) possessed a planar disorder of atomic planes in one of the $\langle 001 \rangle$ directions, though the BCC lattice was preserved as an internal skeleton of their structure. Formation of voids also occurred in the metallic part of the film. These voids were, however, still containing a nano-crystalline phase of the composition close to CrO and having an FCC lattice of about 0.42 nm period. This must be the part of a surface chromium oxide layer, possibly contributing to corrosion resistance of these films [11]. The in-situ annealing experiments suggest, that the structure can be stable up to 400°C for different applications even in harsh environmental conditions, as the surface CrO can serve as a protective layer.

3. Effect of additional alloying elements to HEA [2,3].

The effect of an additional component to the basic HEA alloy (equiatomic CrFeCoNiCu) all having very similar atomic size was further investigated with the main emphasis on the phase formation mechanism in these alloys as the function of the 6th component. Nb, In or Ge were used as alloying elements, due to their different contribution of alloy formation mechanisms. Nb and In have a larger atomic size while Ge has a basically covalent bonding to the other components. Nb, was added in different (5, 10, 15 and 20 at%) quantities to the basic alloy. According to the XRD and TEM measurements the films containing no Nb or 5 at% of Nb were polycrystalline with FCC crystal lattice, the films containing 10, 15 or 20 at. % Nb were amorphous. TEM measurements established that the structure and morphology of the crystalline films (0 and 5 at% of Nb) corresponds to the transition between zone I and zone T in the structure zone model of the thin film growth. The structure is single-phase FCC; the grain size is 2-5 nm. With increasing film thickness columnar grains could be weakly detected, and a slight increase of the crystallite size is also observed. HREM measurements confirmed that the films are dense, homogeneous, free of pores and no detectable foreign phase is present. The HEA films of 10, 15 and 20 at% Nb content are really amorphous, and have homogeneous structure. Nano-crystallites were not detectable even on the level of HREM measurements, where crystallites of 2 nm in size could have been detected [2]. For low solute concentrations of In or Ge, the films also exhibit a single FCC solid solution phase [3]. If the solute concentration exceeds a certain threshold (7 at. % for In and 17 at. % for Ge) the formation of the amorphous phase is favoured. In the case of germanium addition, the crystalline-to amorphous transition was predicted based on Miedema's thermodynamic model [G.J. Van der Kolk, A.R. Miedema, A.K. Niessen, *J. Less-Common Met.* 145 (1988) 1–17]. Ge forms strong covalent bonds with transition metals and this distorts the crystalline lattice leading to the formation of the amorphous phase. In the $\text{In}_x\text{-CoCrCuFeNi}$ system the crystalline-to-amorphous transition could be explained based on Egami's topological theory [T. Egami, Y. Waseda, Atomic size effect on the formability of metallic glasses, *J. Non Cryst. Solids* 64

(1984) 113–134.] for binary alloys though the thermodynamic approach predicted amorphous phase in the 0-20 at. % In concentration region [3]. The ability to predict the phase formation and the influence of non-traditional solute elements on the film growth mode is a valuable contribution to the design of future HEA thin film structures and applications.

This study demonstrates that the ternary alloys could be regarded as binary alloys of the form $(\text{HEA})_{1-x}\text{A}_x$ ($\text{A}=\text{Ge}, \text{In}$ or Nb) and their phase formation can be explained by topological and/or thermodynamic considerations.

4. HEA oxides, nitrides, oxynitrides [7]

HEA films can be further modified by adding the 6th component into the film not from a solid target but from the sputtering gas. In order to achieve this goal N_2 , O_2 or dry air (N_2+4O_2) was added to the sputtering gas in different quantities. Introduction of nitrogen in the vacuum chamber first results in a texture change from $\langle 111 \rangle$ to $\langle 100 \rangle$ at about of 0.1 % of nitrogen. This is attributed to an impurity effect which influences the growth from zone II to zone T [13]. The V-shaped crystallites typical for zone T were observed from TEM images. The metallic FCC lattice can incorporate a certain amount of nitrogen, correspondingly the lattice parameter increases. Then a gradual structural transition seems to occur towards the nitride B1 structure from about of 4 % of nitrogen in the sputtering gas as conformed by lattice parameter and density measurements [7]. Analysis of high resolution TEM images revealed a solid solution of the metals in the cation sites of the nitride lattice. Only some minor inhomogeneity could be observed on the scale of a few nm. The HEA-nitride films have also $\langle 100 \rangle$ preferred orientation which is mainly due to oriented nucleation of the B1 phase as well as the competing (T-zone) growth mechanism from an initial nano-crystalline-amorphous composite of the films in these nitrogen concentrations. Despite the poor ability of most metals to grow stable B1 nitrides, it is remarkable that the ensemble of these metals is able to form this structure [7]. The driving force of this behaviour is an interesting topic for further investigation, this requires not only theoretical calculations but also a wider experimental study to demonstrate the general applicability of this statement. A recent XPS study revealed that from the constituent metals about the half of the Fe, Co and Cr atoms are in nitride bonding when 50% of the sputtering gas is nitrogen, the remaining fractions of these components and Cu as well as Ni remains in the form of the metallic bonding. Beside the HEA-nitride lattice ($a=0.41$ nm) the lattice of the basic HAE metallic alloy can also be faintly detected by electron diffraction ($a=0.36$ nm). As a result, a really nanoscale HEA(metal)-HEA(nitride) stochastic structure forms in which the 1-3 nm regions of different compositions occur randomly and change into each other continuously. The effect of oxygen to the sputtering gas is quite similar to the effect of nitrogen [12]. At low oxygen concentrations (below 1 %) the texture of the film changes to $\langle 100 \rangle$ and the grain size decreases, both are due to the contamination effect caused by the oxygen incorporation and growth in T-zone mode. With increasing oxygen fraction in the sputtering gas transition from the metallic phase to the oxide phase takes place. The components presumably form binary or ternary oxides and the lattice gradually incorporates oxygen. When sufficient oxygen is provided, the resulting thin film forms a stoichiometric oxide (at about 10 % of oxygen in the sputtering gas). This oxide has a B1 structure (FCC, $a=0.42$ nm) with the metal atoms in a solid solution on the cation sites. The solid solution could be confirmed by STEM and EDs measurement, which shows a high degree of homogeneity of all elements in the thin film. The density and the lattice parameter of the possible structures were calculated and coincidence of the B1 structure with the measured values was established. The oxide films grow in clear T-zone structure with a strong $\langle 100 \rangle$ texture [12, 13].

A series of experiments were carried out for depositing a Mn containing HEA (CrFeCoMnNi) alloy in dry air+Ar sputtering gas. The results of structural investigations are summarized in a manuscript, being now in the state of talk-over with co-authors.

We established from the SAED and XRD analysis that the phase composition of the films changes between 20 % and 30 % air in the sputtering gas. Below 20 % air we obtain metallic (solid solution with O and N) crystals/grains of $\langle 100 \rangle$ PO into which a minority oxide phase is epitaxially interlocked resulting in the fragmented grain structure. A slight increase in lattice parameter of the metallic phase can be due to the solute effect (Vegard's law). Above 30 % air the dominating phase is the HEA oxynitride (B1 type, $a=0.42$ nm), interlocked epitaxially with another cubic (FCC) lattice of about 0.51 nm unit cell size (not yet identified).

Besides the broad diffraction peaks belonging to crystalline structure there is a strong diffuse scattering in the diffraction patterns. It is quite evident, that different kinds of disorder can also be present. These fluctuations of the structure on nanoscale are called stochastic structures. We consider this kind of structure to be stochastic in the sense of atomic arrangements and being characteristic for all these films grown in Ar+air as well as grown in Ar+nitrogen or Ar+oxygen sputtering gas. So HEAmetal-N-O stochastic structures must be a typical growth morphology in these films. However, not all kind of diffuse scattering in the diffraction patterns can be attributed to the atomic disorder called as a stochastic system. In addition to the stochastic structure an ordering-disordering phenomenon can also occur on the level of metal(O,N) octahedra as well. The diffuse scattering appearing in the form of straight lines connecting the broad reflections must/may arise from arrangement of larger structural units e.g. the octahedra. These displacements or rotations are arranged on certain crystallographic planes.

To the question on the formation mechanism of these disordered though regular structures an answer can be attempted following the results of interpretation of structural peculiarities of Cu-Ag nanoparticles, grown also by sputtering [1]. There the interlocking Ag/Cu phase separating structure formed by spinodal decomposition. In this case we can suggest the same model. During growth of the film we can imagine that an ideally random structure is deposited which is, however, unstable. Moreover, this unstable structure can have a number of practically equally probable structural variants, having lower energy than the as formed one. So, still during growth, below the growth surface or surface layer of the "ideally" random structure, spinodal decomposition can occur resulting in the stochastic structure and its RUM variations. The result would be a spinodally separated structure with the most easily attainable structures. The structure is essentially metastable or even still unstable, and only the kinetic possibilities will determine where it stops developing further.

Sputtering CrFeMnCoNi in an air, oxygen or a nitrogen atmosphere shows remarkable similarities, such as all cases result in a B1 structure. The differences in incorporation coefficient between the two reactive gases can be linked to the difference in electronegativity between the two elements. Further research is vital in revealing the rationale behind the universal character of both reactive gasses and could give a better understanding about the film growth of these fascinating materials.

5. Mechanical properties of alloy films [2, 5].

The relation between the nanostructure and the mechanical properties of $\text{Nb}_x\text{-CoCrCuFeNi}$ high entropy alloy thin films was explored. With increasing Nb concentration ($x= 0$ to 24 at. %), a transition from a single phase, FCC solid solution to an amorphous phase is observed. At intermediate Nb fractions (5 to 15 at. % Nb) a nanocomposite structure is formed that consists

of nano-size crystallites embedded in an amorphous matrix. The nanocomposite structure leads to an increase in hardness beyond the Hall-Petch breakdown. The shear and Young's moduli decrease with increasing Nb concentration, which is beneficial for the ductility of the film [2].

In a paper published in Hungarian language [5] prospective for IC applications Cu-20 at% Mn alloy films, prepared by DC magnetron sputtering, were investigated. The relation between mechanical properties and micro- or nanostructure of the films was established. The main mechanisms, contributing to increased hardness of the films (above 10 GPa) are the Hall–Petch-effect and hindered operation of Frank–Read dislocation sources [5].

6. Other functional alloys (Cu-Mn, Ni-Mo and $Zr_{44}Ti_{11}Cu_{10}Ni_{10}Be_{25}$ bulk glass)

Cu-Mn films [6]:

Amorphous Cu-Mn thin films (with Mn contents of 50 and 70 at%) were deposited by DC magnetron sputtering on evaporated carbon substrates at room temperature. Carbon substrates were used to model low- κ carbon doped dielectric surfaces in their reaction with Cu-Mn alloy films. The goal was to describe the mechanism of Mn carbide formation and the forming carbide phases. The films were annealed in-situ in the TEM up to 600°C to investigate the thermal stability of the amorphous Cu-Mn films and Mn-carbide formation. The amorphous state was stable below 300 °C, where the films crystallized into Cu(Mn) and α -Mn-based solid solutions. The Cu-based solid solution remained stable up to 600 °C but the Mn-based phases underwent changes. The Mn-carbide phases appeared at 400 °C, accompanied by the disappearance of the α -Mn phase and a decrease in the Mn content of the Cu(Mn) phase. In the temperature range of 400–500 °C, the Mn₂₃C₆ and Mn₅C₂ carbide phases were present. As the temperature increased, more carbon diffused into the film. Hence, the compound with a lower C:Mn ratio (Mn₂₃C₆) disappeared and a new phase with a higher C:Mn ratio appeared, i.e., Mn₇C₃. The Mn₅C₂ carbide crystallites had a lamellar structure and they exhibited Arrhenius-type grain growth in the temperature range of 400–600 °C. The activation energies for Mn₅C₂ growth were 101±20 and 88±22 kJ/mol in the films containing 50 and 70 at% Mn, respectively, thereby indicating that carbide growth was facilitated by higher Mn contents. In addition to carbide formation, surface oxidation also occurred during the annealing process, carried out in 4×10⁻⁷ mbar for about 60 minutes. The results suggest that a thin, uniform barrier layer without carbide formation can be formed on the surfaces of carbon doped oxide (CDO) when sufficient oxygen is available for the full oxidation of Mn within the diffusion distance of the Cu(Mn)/CDO interface and when the diffusion of Mn into the CDO is prevented.

Bulk amorphous alloys [8]

Transmission electron microscopy on the structure of bulk amorphous $Zr_{44}Ti_{11}Cu_{10}Ni_{10}Be_{25}$ alloy was carried out. To exclude or reveal the presence of extremely small (~10 nm) nanocrystals, TEM investigation of the FIB cut samples was carried out together with selected area electron diffraction (SAED) measurements of a highly deformed sample. The TEM image confirmed the homogeneity and amorphous nature of the structure on the ~10 nm-1 µm scale and the SAED pattern verifies that the $Zr_{44}Ti_{11}Cu_{10}Ni_{10}Be_{25}$ bulk metallic alloy preserved the glass state without nanocrystal formation.

Deformation Behaviour of Electrodeposited Ni–Mo Films [10]

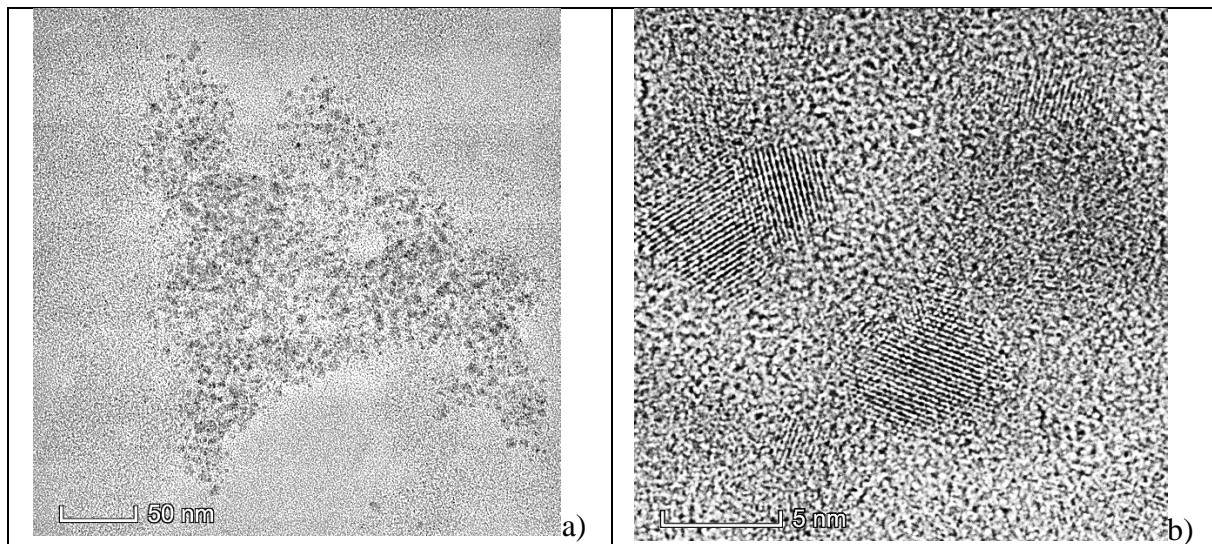
The deformation behaviour of nanocrystalline Ni films deposited with low and high Mo contents was studied by micro-pillar compression test which was performed up to the plastic strain of 0.26.

The film with high (5.3 at. %) Mo concentration had a much larger yield strength (1.3 GPa) than the value obtained for low (0.4 at. %) Mo content (0.35 GPa). This difference was attributed to different factors, namely higher solute hardening, the smaller grain size and higher defect density in the 5.3 at. % Mo sample. In this film, in addition, the formation of nano-twins was observed with a spacing of ~5 nm while no texture of the crystallographic orientations existed. On the contrary in the 0.4 at. % Mo film twinning was not observed, however, a strong $\langle 100 \rangle$ texture existed. These structural differences contributed to the higher yield strength of the 5.3 at. % Mo latter specimen.

The mechanical behaviour of the 5.3 at. % Mo sample showed a continuous softening between the strains of 0.04 and 0.26 after at fast strengthening before this stage. The strain-softening of this film could not be explained by grain coarsening since the average grain size remained about 26 nm during compression. However, a decrease of the twin density during compression was observed by comparing the TEM images taken on the pillars before and after deformation. This detwinning process was thought to be responsible for the observed softening [10].

7. Nano-colloids [15]

Colloid systems are not films; in this sense they are not directly linked to the project. Nevertheless, they are included because they presented a number of properties, interesting also for the formation of films and nanoparticles. Nano-colloids in different ionic liquids were prepared by magnetron sputtering directly into the ionic liquid (IL). Several materials (Fe, Ni, permalloy, C and the basic HEA alloy of the project) were attempted, practically all formed a nano-colloid of different colour. Alloy nano-colloids were composed from alloy particles; no separation of components took place during particle formation in the IL. Some unpublished results on HEA nano-colloids are shown in Fig. 3. The very narrow size distribution is remarkable! The formation mechanism of these particles is not yet clarified.



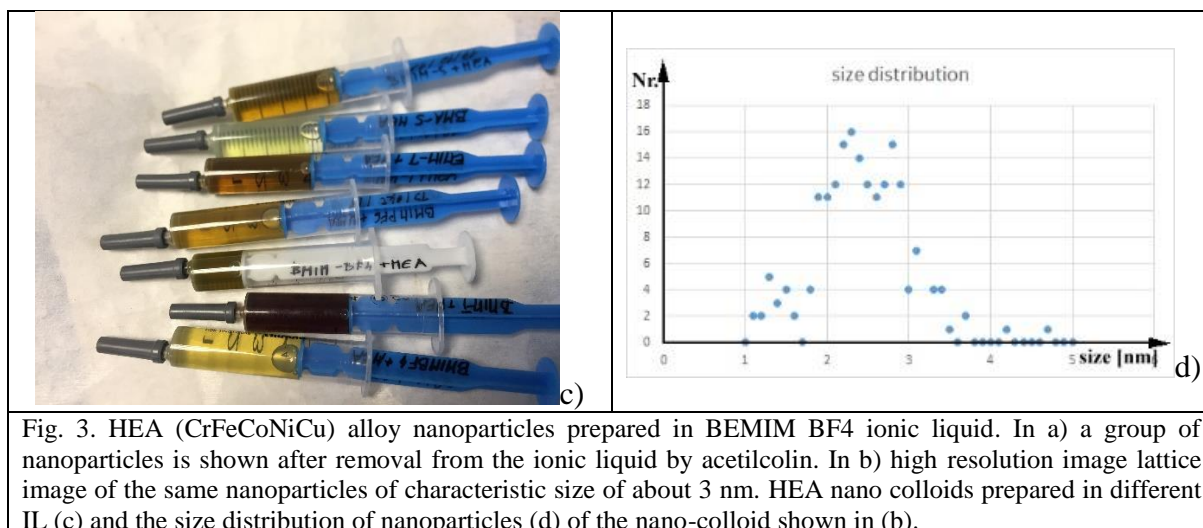


Fig. 3. HEA (CrFeCoNiCu) alloy nanoparticles prepared in BEMIM BF₄ ionic liquid. In a) a group of nanoparticles is shown after removal from the ionic liquid by acetylcholine. In b) high resolution image lattice image of the same nanoparticles of characteristic size of about 3 nm. HEA nano colloids prepared in different IL (c) and the size distribution of nanoparticles (d) of the nano-colloid shown in (b).

Colloids of Ni and Ni-Fe nanoparticles in two imidazolium based ionic liquids (IL) were prepared by magnetron sputtering of nickel and co-sputtering of nickel and iron, respectively, on the surface of the different ionic liquids - [BMIM.BF₆] or [BMIM.Tf₂N]. The nanoparticles were at first characterized by TEM and UV-Vis spectroscopy and then by magnetic measurements using a SQUID magnetometer. Faceted and almost monodisperse nanoparticles of Ni (~10 nm) or Ni-Fe (~12 nm) dispersed in an ionic liquid were formed. The nano-colloids (NCs) were stable for more than 24 months without signs of agglomeration or sedimentation. The metallic nanoparticles exhibited localized surface plasmon resonance in the UV range in all four nano-colloids. The magnetic data were corrected for the diamagnetic contribution of inner-shell electrons of metal atoms. The temperature independent contributions of conduction, delocalized electrons or itinerant charges were determined to reveal superparamagnetic properties of Ni and Ni-Fe NPs in the ILs. A blocking temperature T_B of about 2.5 K was found. Surprisingly, in all the colloids with Ni or Ni-Fe nanoparticles, the effective magnetic moments m_{eff} were higher than in the corresponding bulk metallic materials. In the case of Ni nanoparticles in [BMIM.PF₆] and [BMIM.Tf₂N], m_{eff} of ~3 mB and ~2 mB were determined per Ni atom and for an “average atom” of a Ni-Fe nanoparticle, respectively. The same samples of Ni and Ni-Fe nano-colloids in [BMIM.Tf₂N] were measured again after 32 months and increase in m_{eff} of about 10-20% was found. This provided further evidence of a long-term magnetic stability of IL-based metal nano-colloids. The results of a detailed analysis of magnetic properties of nano-colloids of Ni and Ni-Fe nanoparticles in ionic liquids with imidazolium cation [BMIM], presented in the paper, can be useful for a better understanding of interactions between ionic liquids and metal nanoparticles, e.g. for theoretical modelling.

References

1. G. Radnóczy, E. Bokányi, Z. Erdélyi, F. Misják: Size dependent spinodal decomposition in Cu-Ag nanoparticles ACTA MATERIALIA 123:pp. 82-89. (2017)
2. B.R. Braeckman, F.Misják, G. Radnóczy, M. Caplovicová, Ph. Djemia, F. Tétard, L. Belliard, D. Depla: The nanostructure and mechanical properties of nanocomposite Nb_x-CoCrCuFeNi thin films, Scripta Materialia 139 (2017) 155–158.
3. Braeckman BR, Misják F, Radnóczy G, Depla D: The influence of Ge and In addition on the phase formation of CoCrCuFeNi high-entropy alloy thin films THIN SOLID FILMS 616, pp. 703-710. (2016).

4. F. Misják, K. H. Nagy, M. Čaplovičová, G. Radnóczy, Effect of growth temperature on the structure of CrFeCoNiCu High Entropy Alloy films, oral presentation EVC, Genva, 2018
5. NAGY H. KLÁRA–MISJÁK FANNI: Integrált áramköri alkalmazásra szánt Cu-Mn vékonyrétegek mikroszerkezete és mechanikai tulajdonságai((in Hungarian, English title: Microstructure and Mechanical properties of Cu-Mn thin films designed for Integrated Circuit Applications), *Bányászati és Kohászati Lapok, Kohászat*, 6.) 44-47 (2017).
6. Nagy, K.H; Misják, F: In-situ transmission electron microscopy study of thermal stability and carbide formation in amorphous Cu-Mn/C films for interconnect applications, *JOURNAL OF PHYSICS AND CHEMISTRY OF SOLIDS* 121 pp. 312-318, (2018).
7. Dedoncker, R ; Djemia, Ph ; Radnóczy, G ; Tétard, F ; Belliard, L ; Abadias, G ; Martin, N ; Depla, D: Reactive sputter deposition of CoCrCuFeNi in nitrogen/argon mixtures, *JOURNAL OF ALLOYS AND COMPOUNDS* 769 pp. 881-888. (2018).
8. Kovács, Zsolt ; Ezzeldien, Mohammed; Chinh, Nguyen Quang; Radnóczy, György; Lendvai, János: Nanoindentation measurements on a torsionally deformed $Zr_{44}Ti_{11}Cu_{10}Ni_{10}Be_{25}$ bulk metallic glass, *JOURNAL OF ALLOYS AND COMPOUNDS* 708 pp. 301-307, (2017).
9. Gajdics, BD; Tomán, JJ; Misják, F; Radnóczy, G; Erdélyi, Z: Spinodal decomposition in nanoparticles-experiments and simulation, *DEFECT AND DIFFUSION FORUM* 383 pp. 89-95, (2018).
10. Jenő Gubicza, Garima Kapoor, Dávid Ugi, László Péter, János L. Lábár and György Radnóczy, Micropillar Compression Study on the Deformation Behaviour of Electrodeposited Ni–Mo Films, *Coatings* 10, 205-218; (2020), doi:10.3390/coatings10030205
11. Mohamed Arfaoui, György Radnóczy and Viktória Kovács Kis, Transformations in CrFeCoNiCu High Entropy Alloy Thin Films during in-Situ Annealing in TEM, *Coatings* 10, 60-75; (2020), doi:10.3390/coatings10010060
12. R. Dedoncker, G. Radnóczy, G. Abadias, D. Depla, Reactive sputter deposition of CoCrCuFeNi in oxygen/argon mixtures, *Surface & Coatings Technology* 378 (2019) 124362.
13. P.B. Barna, D. Biro, M.F. Hasaneen,1, L. Székely, M. Menyhárd, A. Sulyok, Z.E. Horváth, P. Pekker, I. Dódony, G. Radnóczy, Cross sectional complex structure analysis is a key issue of thin film research: A case study on the preferential orientation crossover in TiN thin films, *Thin Solid Films* 688 (2019) 137478.
14. Radnóczy, György; Bert, Braeckman ; Diederik, Depla ; Misják, Fanni: Nagyentropiás ötvözet-vékonyrétegek szerkezete (The English title is The Structure of High Entropy Alloy Thin Films.) , *FIZIKAI SZEMLE* 68: 3 pp. 81-85. (2018).
15. Cigaň, A ; Lobotka, P ; Dvurečenskij, A ; Škrátek, M ; Radnóczy, G ; Majerová, M ; Czigány, Z ; Maňka, J ; Vávra, I ; Mičušík, M: Characterization and magnetic properties of nickel and nickel-iron nanoparticle colloidal suspensions in imidazolium-based ionic liquids prepared by magnetron sputtering, *JOURNAL OF ALLOYS AND COMPOUNDS* 768 pp. 625-634, (2018).